PCCP

Accepted Manuscript

ROYAL SOCIETY OF CHEMISTRY

www.rsc.org/pccp

Physical Chemistry Chemical Physics
CREATED USING THE RSC LaTeX PCCP ARTICLE TEMPLATE – SEE www.rsc.org/electronicfiles FOR DETAILS
ARTICLE TYPE www. rsc.org/xxxxxx | XXXXXXXX

Modeling laser induced molecule excitation using real-time time-dependent density functional theory: Application to 5- and 6-benzyluracil†

Attila Bende,*[a] and Valer Toşa[a]

Received Xth XXXXXXXXXX 20XX, Accepted Xth XXXXXXXXX 20XX
First published on the web Xth XXXXXXXXXX 200X
DOI: 10.1039/b000000x

The fully propagated real time-dependent density functional theory method has been applied to study the laser–molecule interaction in 5- and 6-benzyluracil (5BU and 6BU). The molecular geometry optimization and the time-dependent electronic dynamics propagation were carried out using the M11-L local meta-NGA (nonseparable gradient approximations) exchange-correlation functional together with the def2-TZVP basis set. Different laser field parameters like direction, strength, and wavelength have been varied in order to estimate the conditions for an efficient excitation of the molecules. Results show that the two molecules respond differently to the applied laser field and therefore specific laser field parameters have to be chosen for each of them in order to get efficient and selective excitation behavior. It was also found that for the molecular excitation point of view not only the magnitude of the transition dipoles between the involved orbitals are important but also their orientation with respect to the laser field. On the other hand, it was shown that the molecular excitation is a very complex overlap of different one-electron orbital depopulation-population processes of the occupied and virtual orbitals.

1 Introduction

The interaction of different laser pulses with molecules has become a very important topic in current research of femtosecond physics and photochemistry.[1] Photochemical reactions have a great impact on biology, biotechnologies, and daily life, both in bad and good ways. The destructive effects of ultraviolet radiation (UV) on the cellular DNA are strongly connected with photochemical reactions which induce damage of DNA bases.[2] On the other hand the standard photovoltaic effect is directly related to the generation of electron-hole pair in semiconductors or organic molecular systems[3] by electromagnetic radiation. Using laser pulses with femto- and atto-second duration it is now possible to study in detail several processes like multiphoton excitation, high-order harmonic generation[4,5] or real-time electron dynamics.[6]

Transferring laser energy to molecules in a controlled fashion, we might selectively break or create chemical bonds[7] as well as induce different transitions to prepare a desired electronic and/or vibrational state. In all these cases the laser pulse is used to control the dynamics of the atomic and molecular systems.[8,9] Theoretical investigation of laser induced ultrafast processes in molecules using different laser field parameters (polarization direction, strength, pulse duration or angular frequency) can offer us reliable information about how we should set our laser parameters in order to control these ultrafast processes.[10,11]

The linear-response time-dependent density functional theory (LR-TDDFT)[12–15] is an excellent tool to accurately predict properties such as the absorption spectra (vertical excitation energies and oscillator strengths) of molecules.[16] In the linear response regime, the external field is considered as a small perturbation in the sense that it does not completely destroy the ground-state structure of the system. In the real case of the laser-matter interaction, however, one needs to go beyond this linear response and study non-linear excited state dynamics at the femto- and subfemtosecond time scales in order to understand phenomena like nonlinear spectra of single molecules, the nature of photoabsorption, real-time excited state dynamics[17] or transport processes via charge transfer effects,[18] etc.

Using real-time propagation theory instead of linear response one can include nonlinear effects and thus stronger laser field can be applied; on the other hand the framework can directly reveal information about the ultrafast dynamics of electrons and ions during the excitation time. Many successful approaches have been developed to study real-time electron dynamics in realistic systems. They are based on the real-time time-dependent Hartree-Fock (RT-TDHF)[19–22] and den-

† Electronic Supplementary Information (ESI) available. See DOI: 10.1039/b000000x/

[a] *Molecular and Biomolecular Physics Department, National Institute for Research and Development of Isotopic and Molecular Technologies, Donath Street, No. 65-103, RO-400293 Cluj-Napoca, Romania. Fax: +40-264-420042; Tel: +40-264-584037; E-mail: bende@itim-cj.ro*

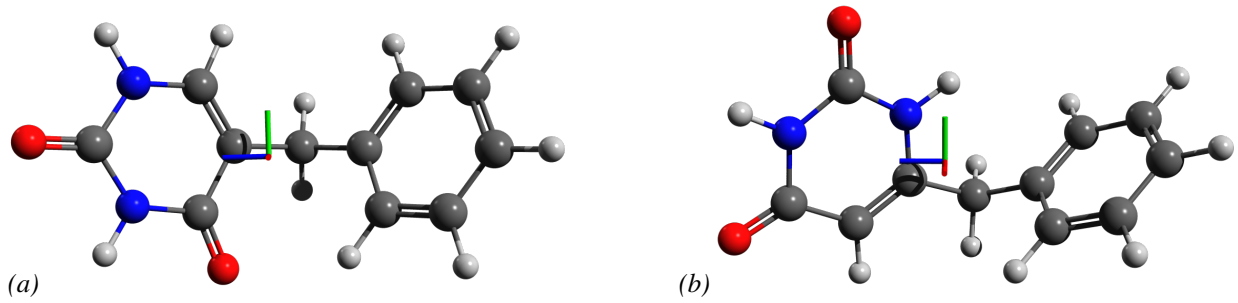

Fig. 1 The optimized geometries of 5-benzyluracil *(a)* and 6-benzyluracil *(b)*. Colors: red for oxygen, blue for nitrogen, gray for carbon and white for hydrogen. The X-, Y-, and Z principal axes are also shown in red, green, and blue lines respectively.

sity functional theory (RT-TDDFT)[19,22,23] within the Born-Oppenheimer approximation. Due to the large progress in the development of efficient exchange-correlation (XC) DFT functionals both static and dynamic electron correlations are more and more covered by the XC functionals and implicitly by RT-TDDFT calculations which becomes suitable to treat molecular electronic states in the presence of the coherent electromagnetic field.

The benzyluracil (BU) can be considered as a model system for the photo-crosslink reaction[24] in biological systems. It contains a benzene ring (which replaces the aromatic part of phenylalanine) and a uracil base which are covalently connected through a methylene bridge. The first and second singlet excited state of the 5-benzyluracil as well as its electronic relaxation pathways have been already studied[25] using the multi-configuration self-consistent Hartree–Fock method. The results show that one can have efficient excitation only if consider transition between the ground and second excited state level. The most likely relaxation pathway starts from this second excited state located at the uracil fragment and through the $S_1 \rightarrow S_2$ conical intersection the molecule reaches its equilibrium geometry of its first excited state. From this S_1 state the molecule can get to its ground state either crossing another energy barrier ($S_0 \rightarrow S_1$ conical intersection) or directly *via* radiation decay. On the other hand, Sun and coworkers[24] have demonstrated that cyclization products derived from the two isomers of the benzyluracil [5- and 6-benzyluracil (hereinafter 5BU and 6BU)] show different reaction yield after the UV irradiation with 2.5 - 3 hour long continuous-wave (CW) irradiation at 254 nm wavelength. They found that the reaction rate is almost two times larger for 5BU than that obtained for 6BU. Using laser pulse instead of the conventional UV-lamp, Micciarelli *et al*[26] have obtained fully photocylized 5,6-benzyluracil product in less than 60 seconds through irradiation with femtosecond UV laser pulses of 200 fs pulse duration (The laser intensity $\approx 1.5{\cdot}10^{11}$ W/cm^2). All these facts suggest us that the photo-induced cyclization strongly depends on the source of irradiation, the intensity of the laser beam, the molecular properties coupled with well-chosen laser field characteristics, etc.

The goal of the present work is to give a detailed description for the real-time electron excitation dynamics of 5- and 6-benzyluracil in the present of laser field. Furthermore, to compare their different molecular responses to the laser field excitation by applying different laser field setup, like frequency or peak intensity. In this way we wait to find the best laser field parameter setup in order to obtain the best absorption yield for the benzyluracil molecular systems.

2 Methodology

2.1 The theoretical framework

The electron population dynamics was investigated using the real time-dependent density functional theory developed by the Manby group[22] and implemented in the MOLPRO 2012.1 quantum chemistry software suite.[27,28] The method solves the time-dependent Kohn-Sham (TDKS) equation:

$$\left[-\frac{\nabla^2}{2} + v_{KS}[\rho](\mathbf{r},t)\right]\varphi_j(\mathbf{r},t) = i\frac{\partial}{\partial t}\varphi_j(\mathbf{r},t) \qquad (1)$$

using the unitary propagation technique with finite time steps[29] and a modified midpoint algorithm is used for better efficiency.[21] In eq. (1) v_{KS} is the Kohn-Sham effective potential and $\varphi_j(\mathbf{r},t)$ are the single-particle orbitals. The initially occupied $\varphi_j^0(\mathbf{r})$ single-particle orbitals are considered as the initial conditions ($\varphi_j(\mathbf{r},t_0)$). (for more details see Ref. 22.)

The molecular orbitals are expanded in a basis of time-independent atomic orbitals χ_μ with time-dependent coefficients $c_{\mu j}(t)$:

$$\varphi_j(t) = \sum_\mu c_{\mu j}(t)\chi_\mu \qquad (2)$$

and the product of the time-dependent coefficients gives the density matrix:

$$\rho_{\mu\nu} = \sum_j c_{\mu j}(t)c_{\nu j}^*(t) \qquad (3)$$

The interaction of the molecular system with the laser field is taken into account through the relation between the time-dependent Fock operator $\mathbf{F}(t)$ and the sum of the field-free Fock operator $\mathbf{F}_0$ and the dipole matrix $\mathbf{D}$ taken in the direction of the laser field $\mathbf{e}(t)$:

$$\mathbf{F}(t) = \mathbf{F}_0 + \mathbf{D}\mathbf{e}(t) \quad (4)$$

Orbital occupation numbers, $n_k(t)$, are calculated by projecting the time-dependent density $\rho(t)$ matrix onto the initial, field free single-particle orbitals $\varphi_j(\mathbf{r},t_0)$:

$$n_j(t) = \varphi_j^{\dagger}(\mathbf{r},t_0)\rho(t)\varphi_j(\mathbf{r},t_0) \quad (5)$$

See Ref 22 for a detailed description of the solution of the RT-TDHF (RTTDDFT) equation and the capability of the real-time dependent program module implemented in MOLPRO.

The current version of the TDHF/TDKS module could not be used together with hybrid DFT functionals were both the exchange–correlation (XC) functional part and the HF exchange are used simultaneously, it works only with pure (local) XC functionals.

2.2 Computational details

For the real case we have considered the M11-L[30] local meta-NGA (nonseparable gradient approximations) XC functional as a part of the v_{KS} Kohn-Sham effective potential from eq. (1), together with the def2-TZVP[31] basis set. The M11-L XC functional employs dual-range local exchange to give highly accurate results (for a local functional) for both single-configurational and multiconfigurational molecules and has good performance for Rydberg as well as for valence excited states.[32] Usually the performance for the charge-transfer excitations remains beyond the capability of local functionals, but M11-L gives relatively good performance also for this case in comparison with other local XC functionals.[32]

During this investigation it was necessary to perform benchmark calculations considering also the M11[33] hybrid meta-GGA functional and the Tamm-Dancoff[34] approximation for the TDDFT scheme, implemented in the GAUSSIAN09[36] program package. This benchmark study also includes the so-called Tozer's[37] lambda (Λ) diagnostic test, which measures the spatial overlap of the electron–hole pair orbitals involved in the excitation description. Numerical values of Λ near zero describe long-range excitations, values near unity indicate short-range or localized excitations, while values in the middle range interval describe charge-transfer excitations. On the other hand, XC functionals for which a certain transition gives $\Lambda < 0.3$, might be affected by errors and underestimates the excitation energy.[37]

The total propagation time was considered $\approx$ 23 fs with the time-step of 0.0048 fs (the number of steps = 4800). We limit on this time scale in order to keep the conditions for the rigid-body approximation assumed in the case of our molecular systems. The laser field pulse envelope has set in the *trap* form which grows from zero in one field oscillation, stays constant for n periods (in our case n = 30) and then decays to zero in one period.

The vertical excitation energies and absorption spectra were obtained using the linear response TDDFT module implemented in the MOLPRO package. In this module the electron correlation integrals are calculated using the density-fitting technique,[35] while the exchange-correlation kernel is approximated by the adiabatic local density approximation.

The molecular graphics (figures) were created using the AVOGADRO[38] software.

3 Results and Discussion

Equilibrium geometries of 5- and 6-benzyluracil were optimized using the M11-L local XC functionals together with def2-TZVP basis set. The optimized structure of 5- and 6-benzyluracil are presented in Figure 1. The XYZ principal axes of the molecules are also indicated on Figure 1 with red, green and blue colors, respectively. Setting the electric field along the *X*, *Y*, and *Z* principal axes help us to describe the excitation modes in the two molecules. The electric field oriented along the *X* axis corresponds to an excitation perpendicular to the molecular planes of the fragments, while the field direction along *Y*axis is typical for the uracil and benzene fragments excitation; finally the laser field polarization oriented along *Z* axis overlaps with the direction of the charge transfer excitation between the fragments.

3.1 The vertical excitation and the UV-absorption spectra

The vertical excitation energies of the first four singlet excited states for 5BU and of the first five singlet excited states for 6BU molecular systems, their oscillator strengths, the corresponding transition dipole orientation with respect to the *Z* axis and the one-electron orbital transitions are collected in Table 1.

The transition between S_0 and S_1 states of the 5BU system involves excitations from HOMO-2, HOMO-1, and HOMO to LUMO as well as between the HOMO-1 occupied and the LUMO+2 virtual orbital. The magnitude of the oscillator strength of the transition is 0.027. The second transition ($S_0 \rightarrow S_2$) is a very weak excitation, its oscillator strength is only 0.0008 and includes similar one-electron orbital transitions as one was obtained for the previous case. The third, $S_0 \rightarrow S_3$ excitation incorporates one-electron transitions between the four highest occupied orbitals and the LUMO virtual orbital. In case of 6BU molecular system, the first and third excited states

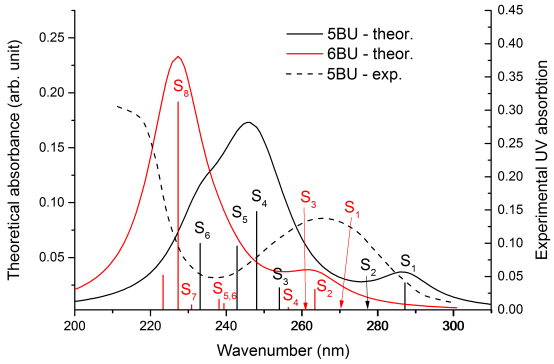

Fig. 2 Absorption spectra of 5BU and 6BU. Experimental spectra (dashed lines – taken from Ref.[26]) are shown together with LR-TDDFT/M11-L/def2-TZVP convoluted spectra (continuous lines). The vertical excitation energies (resonances) are represented by bars with a height corresponding to their oscillator strength.

have weak oscillator strengths, only the transition between the ground and the second excited states has a considerable efficiency. In this case we found one-electron excitation from the two highest occupied orbitals (HOMO and HOMO-1) to the three lowest unoccupied orbitals (LUMO, LUMO+1 and LUMO+2). In order to better understood the nature of the excited states, the orientation of the transition dipole with respect to the Z axis was also calculated. Accordingly, those transitions which exhibits small angle deviation as compared with the Z axis direction could be considered as dominant charge-transfer excitations, while in cases when this angle is relatively larger both charge transfer and fragment (uracil $\rightarrow$ uracil and benzene $\rightarrow$ benzene) are present.

The experimental UV spectra have been already measured by Micciarelli *et al.*[26] They found two peak domains centered around the wavenumber values of 210 nm and 265 nm. They show that the calculated bands give a systematic blue shift ($\approx$ 20 nm), but the overall agreement between theory and experiments is sufficient to allow an unequivocal assignment of the electronic transitions. The experimental[26] for 5BU and the computed UV absorption profiles for the 5BU and 6BU molecules, respectively, are reported in Figure 2 (respectively with dashed lines and continuous lines). Comparing the theoretical UV absorption spectra for 5BU and 6BU systems one could observe that there are significant differences between their vertical excitation energy positions in the spectra. For example, the first excited state of the 5BU molecule is resonant with the 287 nm wavelength, while the similar electronic state of 6BU shows a value of 270 nm. Furthermore, we have found that their oscillator strengths are also different. In the first case we have a reasonable absorption intensity, but for the 6BU case the $S_0 \rightarrow S_1$ excitation shows a very weak transition.

Table 1 Vertical excitation energies (in eV as well as in nm in parenthesis), their oscillator strengths (and the transition dipole orientation with respect to the Z axis) and the corresponding orbital transitions for 5-benzyluracil (5BU) and 6-benzyluracil (6BU) molecular systems.

State	Excit. energy	Oscillator strength	One-electron orbital transition	Proc. (%)
5BU				
S_1	4.32	0.0270	HOMO-2 $\rightarrow$ LUMO	(4%)
	(287)	13.9°	HOMO-1 $\rightarrow$ LUMO	(39%)
			HOMO $\rightarrow$ LUMO	(55%)
S_2	4.46	0.0008	HOMO-2 $\rightarrow$ LUMO	(76%)
	(278)	24.5°	HOMO-1 $\rightarrow$ LUMO	(20%)
			HOMO $\rightarrow$ LUMO	(2%)
S_3	4.88	0.0225	HOMO-3 $\rightarrow$ LUMO	(78%)
	(254)	37.2°	HOMO-2 $\rightarrow$ LUMO	(8%)
			HOMO-1 $\rightarrow$ LUMO	(6%)
			HOMO $\rightarrow$ LUMO	(4%)
S_4	4.99	0.0919	HOMO $\rightarrow$ LUMO+2	(21%)
	(248)	40.4°	HOMO $\rightarrow$ LUMO	(18%)
			HOMO-3 $\rightarrow$ LUMO	18%)
			HOMO-1 $\rightarrow$ LUMO	(16%)
6BU				
S_1	4.59	0.0019	HOMO $\rightarrow$ LUMO	(6%)
	(270)	18.1°	HOMO $\rightarrow$ LUMO+1	(93%)
S_2	4.71	0.0210	HOMO $\rightarrow$ LUMO	(54%)
	(263)	22.0°	HOMO $\rightarrow$ LUMO+1	(6%)
			HOMO $\rightarrow$ LUMO+2	(38%)
S_3	4.74	0.0007	HOMO-1 $\rightarrow$ LUMO	(98%)
	(261)	37.5°		
S_4	4.84	0.0045	HOMO-1 $\rightarrow$ LUMO+1	(98%)
	(256)	9.7°		
S_5	5.18	0.0082	HOMO-1 $\rightarrow$ LUMO+2	(55%)
	(240)	8.6°	HOMO-2 $\rightarrow$ LUMO	(40%)

Setting the laser frequency to 254 nm one might probably excite the third excited state of 5BU and partially, the second excited state of 6BU. As one can see in Figure 2, for this laser frequency, the UV absorption for 5BU is stronger than that for 6BU.

Our previous investigation[25] reveals that the first excited (S_1) state transition has a $n\pi^*$ character and covers the fragment excitations which develops a very small oscillator strength ($f = 0.003$). At the same time, significant oscillator strength ($f = 0.571$) was obtained for the $S_0 \rightarrow S_2$ ($\pi\pi^*$) transition, which describes the charge transfer excitation from the uracil to the benzene fragment. On the contrary, linear response TDDFT yields a stronger oscillator strength for $S_0 \rightarrow S_1$ transition and a smaller one for the $S_0 \rightarrow S_2$ transition. This

could happen due to the poorer description of the excited states by the M11L local XC functional used by TDDFT method compared to that of non-local XC functional (for example, M11[30]) or multireference CASSCF. To unravel the discrepancy in the magnitude of the oscillator strength of the $S_0 \rightarrow S_2$ ($\pi\pi^*$) transition we have performed benchmark TDDFT calculations considering the M11 XC hybrid meta-GGA functional and Tamm-Dancoff approximations. Our conclusions is that the strong oscillator strength value ($f = 0.215$) for $S_0 \rightarrow S_2$ ($\pi\pi^*$) transition is obtained only when the both approximations are taken into account. Moreover, performing the so-called Tozer's[37] lambda diagnostic test implemented in the GABEDIT[39] the difference between the M11 and M11L local XC functional becomes more conclusive. For the first three excites states the Λ values are 0.43, 0.62 and 0.62 for M11, and 0.64, 0.24 and 0.95 for M11L. One can observe that M11L gives smaller Λ value for the second excited state which means poorer description for the $S_0 \rightarrow S_2$ transition.

3.2 Excitation of 5BU

The real-time electronic dynamics for 5BU have been computed using an oscillating (laser) field of strength E_{max} = 0.005 a.u. (laser intensity = $8.76 \cdot 10^{11}$ W/cm^2) and wavelength of λ = 254 nm, applied in the *X*, *Y*, or *Z* directions, as defined by the principal axes of the molecule. In Figure 3 we present the orbital population dynamics of different HOMO and LUMO orbitals, as well as the sum of the last eight occupied orbitals depopulation and the first nine unoccupied orbitals population on a time scale of 23 fs. When the oscillating field is set along the *X* axis (red color in Figure 1) the electronic excitation shows the following characteristic: both the HOMO and HOMO-1 orbitals are depopulated by about the same extent and the electrons from these orbitals are excited to the LUMO virtual orbital. In this way we have two major transitions HOMO-1 $\rightarrow$ LUMO and HOMO $\rightarrow$ LUMO completed with a third weaker HOMO-3 $\rightarrow$ LUMO transition. Counting the total electron transition we found that the yield of excitation along the *X* axis is less than 0.1*e* in 23 fs. The full list of figures containing the last seven occupied orbitals and the first eight unoccupied (virtual) orbitals are given in Figure S1 of ESI†.

If the laser electric field is set along the *Y* or *Z* directions, the pictures of one-electron orbital excitations are almost the same (See the second and third rows of Figure 3). The only significant difference is in the yield of the electron transition between the HOMO and LUMO orbitals, which is somewhat larger for *Z* direction than for *Y* direction and both are much larger than the yield seen in *X* direction. The laser field promotes electrons mainly from HOMO-3, HOMO-1 and HOMO to LUMO orbital and to lesser extent to LUMO+1 and LUMO+2 virtual orbitals. It is interesting to note that the total electron depopulation of the occupied orbitals ($\sum_{i=0,7} 2 - HOMO\text{-}i$) is different from the total electron population of virtual orbitals ($\sum_{i=0,9} LUMO\text{-}i$). This suggests that there should be higher virtual orbitals which are involved in the excitation scheme. Similar behavior was observed in our previous work[25] when the EOM-CCSD one-electron orbital excitation scheme was analyzed. On the other hand, one can observe that electron excitations to LUMO+3,...,LUMO+9 virtual orbitals is very weak, which suggest us that the transition of the valence electrons to Rydberg molecular states is absent.

As a first conclusion, we can say that a significant electron excitation is obtained when the laser field is set along the *Y* and *Z* axes, while for the *X* direction we have a small amount of electron transfer.

To better understand the nature of the excitation along the three principal axes, we have computed similar electron excitation dynamics for the isolated uracil, by keeping its orientation as in 5BU. The results show a similarity with the 5BU case that is a weak excitation along the *X* axis, but significant electron excitations along *Y* or *Z* directions. However, for the isolated uracil the occupation number along the *Y* direction was almost two times larger than along the *Z* direction (*Y*: 0.40*e* and *Z*: 0.23*e*). The same occupation numbers for 5BU are *Y*: 0.53*e* and *Z*: 0.80*e* which means that we have an extra contribution to the yield along the *Z* axis coming from the charge transfer from the uracil to the benzene fragment, which is present in 5BU.

It is interesting to compare the results given by the linear-response TDDFT and the real-time TDDFT theories. First, all four transitions (HOMO-3 $\rightarrow$ LUMO, HOMO-2 $\rightarrow$ LUMO, HOMO-1 $\rightarrow$ LUMO and HOMO $\rightarrow$ LUMO) obtained for the $S_0 \rightarrow S_3$ excitation (Table 1) using the 254 nm wavelength are also present in the HOMO and LUMO orbital population graphs (Figure 3). However, if one compares the relative contribution of different orbital transitions we note major differences. For example, for the strong contribution (78%) of the HOMO-3 $\rightarrow$ LUMO transition estimated by the linear-response theory corresponds a very small HOMO-3 depopulation; on the other hand HOMO-1 and HOMO depopulations and the LUMO population are significant only in the real-time TDDFT description (See Figure S2 of ESI†). Moreover, LUMO+1 and LUMO+2 orbital populations in the real-time case are not present as orbital transitions in the linear response case. A possible explanation could be the fact that we have used relatively short laser pulse which has broad spectral width. Indeed, for 23 fs long pulse centered at the 254 nm the full width at half maximum (FWHM) is 21 nm, which means that also the S_4 state might be involved in the excitation. Repeating the calculation for a longer pulse duration (60 fs having 8 nm FWHM spectral width) we found practically the same behavior in the excitation dynamics of orbitals: the HOMO-1 and HOMO keep the same depopulation

progress, while the HOMO-3 and HOMO-2 orbital depopulations remains very low. Similar behavior was seen for LUMO, LUMO+1 and LUMO+2 population processes. As a conclusion we can state that the spectral width of the femtosecond laser pulse does not play here a role in the picture of orbital dynamics for the 5BU.

To analyze further the excitation mechanism described by the two theories we show in Figure 4 the theoretical UV-spectra obtained with the linear-response method and the Fourier transform of the dipole moment after the pulse was switched off. Even if the dipole moment spectra still contains the frequency of the excitation pulse there is a good overlap between the absorption spectra obtained with the two theories. This fact tells us that the two theories describe well the excited states in the field-free molecule. However, the excitation mechanism in the presence of the laser field might happen differently than that suggested by the linear-response theory. It is worth to note that the strong excitation seen along the Z axis is in clear connection with the shapes and localization of the orbitals involved in transitions. Indeed, if we analyze these for HOMO-1, HOMO and LUMO orbitals (See Figure S1 of ESI†) we see that a transition between HOMO-1 or HOMO to LUMO orbital involves a charge-transfer-type excitation in the presence of an electric field oriented along the Z axis. In order to maximize the interaction between the molecule and the laser field we conclude that not only the magnitude of the transition dipoles between the involved orbitals are important but also their orientation with respect to the electric field. On the other hand, the angle of the transition dipole moment for $S_0 \rightarrow S_3$ excitation with the Z axis is 37.2°, as seen in Table 1. This indicates that the $S_0 \rightarrow S_3$ transitions includes not only charge-transfer excitation from one fragment to other (lying in Z direction), but also the fragments excitation, which take place mostly along Y direction. A laser field oriented along the Z axis will overlap with the direction of the charge transfer excitation therefore only this component of the $S_0 \rightarrow S_3$ transitions will be excited.

3.3 Excitation of 6BU

Using the same oscillating field setup, applied again for X, Y, and Z directions we have computed the same orbital population transfer dynamics for 6BU. In Figure 5 we present the orbital population dynamics of different HOMO and LUMO type orbitals, as well as the sum of the last eight occupied orbitals depopulation and the first nine unoccupied orbitals population during the time scale of 23 fs, and assuming the same laser pulse shape. One can see that for a polarization direction of the laser field along the X direction, almost no excitation can be observed. The total amount of fractional electron excitation after 23 fs irradiation is only $0.027e$. Changing the field direction along the Y axis, a relatively stronger excitation was obtained, the total amount of fractional electron excitation after 23 fs irradiation being $\approx 0.24e$. The most relevant one-electron orbital excitations are the HOMO $\rightarrow$ LUMO and HOMO $\rightarrow$ LUMO+2 transitions. Finally, the strongest excitation was found when the laser polarization direction was set along the Z axis. For this case, the total amount of fractional electron excitation at the end of the laser pulse is $\approx 1.1e$. The one-electron transition are dominated by the HOMO $\rightarrow$ LUMO ones, but also transitions from HOMO-1, HOMO-2 and HOMO-3 to LUMO+1 and LUMO+2 orbitals should be noted. Analyzing the spatial configuration of the one-electron orbitals we observe that HOMO $\rightarrow$ LUMO and HOMO $\rightarrow$ LUMO+2 transitions involve both the uracil $\rightarrow$ uracil and the uracil $\leftrightarrow$ benzene charge transfer excitations, while the HOMO $\rightarrow$ LUMO+1 and HOMO-1 $\rightarrow$ LUMO+1 transitions involve only charge transfer excitations. The orbital shapes containing the last seven occupied orbitals and the first eight unoccupied (virtual) orbitals are listed in Figure S3 of ESI†.

Similarly to the case of 5BU, we have investigated electron excitation dynamics for the isolated uracil by keeping the uracil orientation as in 6BU. Setting the laser field polarization along the uracil X axis we found insignificant fractional electron depopulation of the occupied orbitals, as we found for 6BU. If the polarization of the laser field is set in the direction of Y or Z axes a significant excitation yield was obtained (Y: $0.23e$ and Z: $0.22e$). We note an important increase of excitation efficiency for the 6BU along the Z axis from the value of $\approx 0.22e$ fractional electron excitation obtained for isolated uracil to almost $0.80e$ for 6BU. This can be explained by the presence of the charge transfer excitation which is induced by the laser field polarized along the Z axis. The amount of the transferred charge during the 23 fs irradiation time is around $0.57e$.

As we have mentioned in case of the 5BU system the 23 fs long pulse centered at 254 nm wavelength has a FWHM of 243.5 – 264.5 nm, which in case of 6BU includes the $S_0 \rightarrow S_3$, the $S_0 \rightarrow S_4$ excitations and also partially the $S_0 \rightarrow S_5$. The real-time propagation results presented in Figure 5, show that mainly HOMO-1 and HOMO orbitals are depopulations and LUMO and LUMO+2 virtual orbitals are populated. This excitation picture does not fully correspond to the orbital transitions found in the linear-response case, where mostly the HOMO-1 are depopulated and LUMO, LUMO+1, LUMO+2 populated. As for 5BU, we have performed a new real-time propagation calculation by setting a longer pulse duration (60 fs). In this way, the FWHM is reduced to the 8 nm, which limits the excitation of the 6BU to the $S_0 \rightarrow S_4$ transition. The result obtained for this case are presented in Figure S4 of ESI†. As it can be observed in the figure, we have significant orbital depopulation for the HOMO and to a lesser extent for the HOMO-3 and HOMO-2. The population for LUMO has a fast increase in the time interval of 0 – 28 fs and a stagnation

effect until the end of the pulse. Again we compare the total depopulation of the last eight HOMO orbitals with the total population of the first nine LUMO orbitals and we observe an increasing difference between them especially after the 28 fs irradiation time. This difference indicates that there are higher virtual orbitals which might be populated during the excitation. Indeed, performing a detailed analysis of the shape of higher virtual orbitals we have identified the LUMO+17 and possibly also LUMO+21 and LUMO+23 orbitals (See Figure S5 of ESI†)as candidates in the excitation process.

As for 5BU, we have compared the mechanism of the excitation described by the linear-response and the real-time propagation theories. Accordingly, we have compiled together on the same graph (See Figure 6) the theoretical UV-spectra obtained with the linear-response method and that of the Fourier transform of the dipole moment after the pulse was switched off. The theoretical UV-spectra (blue-line) has a main large spectral peak at 227 nm wavelength (corresponding to S_8 excited state) completed with a much smaller spectral ridge given by the $S_0 \rightarrow S_2$ excitations. The Fourier transform of the dipole moment intensity matches very well with the UV main peak, but this band shape is perturbed by another broad peak given by the laser excitation frequency. This relatively good agreement proves us that also for 6BU the two theories describe well the excited states in the absence of the laser field and that the excitation mechanism in the presence of an external laser field might have a different behavior than that given by the field-free linear-response theory.

3.4 5BU versus 6BU

As we have already seen, laser field polarization oriented along the *X*, *Y*, or *Z* directions can induce various excitation schemes. For 5BU we have efficient excitation if one sets the electric field along the *Y* or *Z* directions (with a slightly better performance for the second case), while for the 6BU only the field along the *Z* direction can induce considerable electron excitation. We have previously shown[25], that for the 5BU system, the energy of the laser field is mainly absorbed by the uracil fragment or more precisely by the C^4=O group of the uracil. If one compares the orientation of the C^4=O bond and the field directions which have given efficient excitations (*Y* and *Z* axes) one can conclude that a more efficient excitation would be obtained if the laser field direction would be set along the *YZ* direction which coincide with the direction of the dipole moment formed along the C=O bond. Accordingly, we have further performed similar calculations for both *YZ* and its perpendicular direction -*YZ*. The results of the occupied and virtual orbital populations for 5BU along the *YZ* and -*YZ* field directions are presented in Figures S6 and S7, respectively, of ESI†. Analyzing the total fractional electron excitation for both directions, a significant increase of laser field absorption was obtained for the *YZ* direction ($\approx 1.3e$) compared with the *Y* ($\approx 0.55e$) and the *Z* ($\approx 0.8e$) directions, while for the perpendicular case of -*YZ* direction the excitation becomes extremely inefficient (only $0.2e$). The similar result along the same *YZ* and -*YZ* field directions for the 6BU system are presented in Figure S8 and Figure S9, respectively, of the same of ESI†. As we can observe in Figure 1 the orientation of the C^4=O bond in 6BU system is rotated with almost 90°compared with the 5BU case. This fact suggests that one would obtain exactly the opposite case, namely, strong laser field absorption along the -*YZ* direction and much weaker absorption along the *YZ*. Indeed, the total fractional electron excitation along the -*YZ* direction is $\approx 1.6e$, while for the *YZ* case $\approx 0.25e$ was obtained. Comparing the excitation efficiency for 5BU along the *YZ* direction with that of 6BU along the -*YZ*, one can conclude that 6BU could be excited with a slightly better result using the 254 nm excitation wavelength. This fact is also demonstrated with the more efficient charge transfer excitation obtained for the 6BU case ($\approx 0.22e$ transferred charge in the 5BU case *versus* $0.57e$ for 6BU case). To better understand the differences between the excitation behavior of 5BU and 6BU molecular systems we have compiled a multiple plot (See Figure S10 of ESI†) with occupation numbers for HOMO-2, HOMO-1, HOMO, LUMO, LUMO+1, and LUMO+2 orbitals generated by the laser field applied along the *Z* axis. It can be observed that dominant processes, like the HOMO orbital depopulation and the LUMO virtual orbital population, after a 11–13 fs irradiation become more intense for the 6BU case than that for the 5BU. Lower occupied orbital (HOMO-2 and HOMO-1) depopulations and higher virtual orbital (LUMO+1 and LUMO+2) populations have moderate intensities, and which in some cases are stronger for 5BU and in other cases for 6BU.

3.5 The influence of the laser frequency

An interesting issue is obviously the dependence of the excitation dynamics on the frequency of the oscillating laser field. For this reason, besides the results obtained at 254 nm laser wavelength we performed further real–time electronic dynamics for three more laser wavelength values: 240 nm, 270 nm and 290 nm for the laser field applied along the *Z* direction. The fractional electron population for the more relevant occupied (HOMO-2, HOMO-1 and HOMO) as well as virtual (LUMO, LUMO+1 and LUMO+2) orbitals for the 5BU system obtained with four different laser frequencies are presented in Figure S11 of ESI†, while the total fractional electron depopulation of the first seven occupied orbitals is shown in Figure 7. After 23 fs irradiation time we have significant one-electron excitation for all frequency values, except for the longer 290 nm wavelength where we have obtained only a very small effect, which looks saturate after a few fs time-

scale. It is also important to note that after 10 fs irradiation time the slope of the curve obtained with 240 nm wavelength becomes smaller than those obtained for 254 nm and 270 nm. These two frequency values are also close to the UV absorption peaks presented in Figure 1. If one individually analyzes the one-orbital excitations one can observe, for 240 nm case, a significant HOMO-2, HOMO-1 and HOMO orbital depopulations which are mostly transferred to LUMO+1 virtual orbital. For 270 nm we note strong transition only for HOMO $\rightarrow$ LUMO excitation. Apparently, it looks that the excitation curve for 270 nm shows similar elevation, and thus similar absorption efficiency, as it is for 254 nm and 240 nm cases. However, if we carefully analyze also the *Y* component contribution (See Figure S12 of ESI†) we could observe that this component for the 270 nm is almost missing and the effective absorption efficiency given by the contribution of both *Y* and *Z* directions is smaller than those obtained for the 240 nm and 254 nm values. Performing similar studies for the 6BU case, relatively small laser field absorption efficiencies are observed for 270 nm and 290 nm frequency values (See Figure 8 and Figure S13 of ESI†). This fact is in a very good agreement with results which derive from the TDDFT UV absorption spectra (See the line for 6BU in Figure 1), where the absorption line rapidly decays to zero. On the other hand the slope of the curve for the 240 nm frequency excitation is a bit steeper than for 254 nm, which is again in agreement with the UV absorption intensities for the above mentioned frequency values founded with the TDDFT method.

3.6 The influence of the laser intensity

An important parameter which can be easily set experimentally for the laser field is the laser field intensity. Accordingly, in addition to the reference value of 0.005 a.u. we have chosen two more values for the field strength (0.002 a.u. and 0.008 a.u.) in order to reveal the influence of the field intensity on the orbital excitation. These three values for the electric field strength (0.002, 0.005, and 0.008 a.u.) corresponds to peak intensities of $1.40{\cdot}10^{11}$, $8.76{\cdot}10^{11}$ and $2.24{\cdot}10^{12}$ W/cm^2. In Figure 9 we have compiled the total fractional electron depopulation of the first seven occupied orbitals for 5BU using the three laser intensities, while the field direction was set along the direction of *Z* axis. The same results for 6BU are shown in Figure 10. As it could be observed, the intensity value of $1.40{\cdot}10^{11}$ W/cm^2 induce relatively small depopulation-population effects of the occupied-virtual orbitals for both 5BU and 6BU cases, while for the $8.76{\cdot}10^{11}$ W/cm^2 intensity value we have obtained steadily increasing depopulation-population rate. During the 23 fs time-scale, if one applies a higher intensity value ($2.24{\cdot}10^{12}$ W/cm^2) this increasing tendency remains quite similar for 6BU, but shows a saturation followed by a small decreasing for 5BU. In both cases the peak intensity value of $2.24{\cdot}10^{12}$ W/cm^2 induces almost a double amount of fractional electron excitation ($\approx 1.25e$ for 5BU and $\approx 2.2e$ for 6BU) than that obtained for $8.76{\cdot}10^{11}$ W/cm^2 ($\approx 0.7e$ for 5BU and $\approx 1.2e$ for 6BU). If one analyses the different occupied and virtual one-electron orbital behavior, as is presented in Figures S14 and S15 of ESI†, a much more complex picture of depopulation-population process emerges. In case of 5BU, the most significant one-electron orbital depopulations are obtained for HOMO-1 and HOMO occupied orbitals, from which electrons are transferred mostly to the LUMO virtual orbital. In case of HOMO-1, after 14 fs the depopulation process stops and saturation effect is observed, while the depopulation process of HOMO lasts for 19 fs and then starts to decrease. Depopulation of HOMO-2 and population of LUMO+1 and LUMO+2 have much lower contributions. In case of 6BU, the strongest transition is the HOMO $\rightarrow$ LUMO excitation, where the population of LUMO increases for 15 fs than it starts to decrease. This decrease is mainly compensated by the population increasing of LUMO+1 and LUMO+2 virtual orbitals. An important contribution to the magnitude of the electron depopulation can be also observed for HOMO-2 occupied orbital.

4 Summary and conclusions

We have investigated the real-time electron dynamics in the case of laser induced molecular excitation of 5- and 6-benzyluracil (5BU and 6BU) molecular systems by using real-time time-dependent density functional theory method. The basic laser field parameters were set as: 254 nm for the laser wavelength, $2.24{\cdot}10^{12}$ W/cm^2 peak intensity and 23 fs as the pulse duration.

A first important finding is that there are significant differences in the case of the efficiency of the laser field absorption applied along the three principal axes of the molecules. 5BU can be easily excited if one applies the laser field along the *Y* or *Z* axes, while 6BU could efficiently absorb only if the field is applied along the *Z* axis. The absorption efficiency can be increased if the polarization of the laser field is not set along one of the principal axes, but through the combination of different vector directions. Accordingly, for 5BU we have obtained the highest excitation efficiency if the field is oriented along the *YZ* direction, while 6BU gives the highest yield of absorption for the -*YZ* direction, which is perpendicular on the previous direction. This fact clearly demonstrates the necessity of the molecular alignment before the molecular system is being excited by a laser field. On the other hand, larger charge transfer effect was obtained for the 6BU case than that of 5BU when the laser field polarization is set along the *Z* axis.

We have shown that there is a relatively good agreement between the theoretical UV-spectra obtained with the linear-response method and the Fourier transform of the dipole mo-

ment calculated by real-time propagation theory. On the other hand we obtained different orbital transitions predicted by in the linear-response and in the real-time propagation excitation which suggests the idea that the excitation mechanism in the presence of the laser field shows different behavior than that given by the field-free linear-response theory. The strong correlation seen between the orbital shapes and field direction lead us to conclude that not only the magnitude of the transition dipoles between the involved orbitals are important but also their orientation with respect to the electric field.

Choosing four different wavelengths (240 nm, 254 nm, 270 nm and 290 nm) for the laser pulse a selective behavior for the molecular excitation was observed. Similarly with the theoretical UV spectra obtained using the TDDFT theory, the excitation wavelength of 290 nm is not able to produce significant changes in the electronic structure of the molecules. However, the wavelength of 270 nm could selectively excite only the 5BU molecule against the 6BU and only in the *Z* direction, the excitation along the *Y* axis having a very small absorption rate. For lower wavelengths values the selectivity between 5BU and 6BU cases vanish and we obtain a relatively complex picture of one-electron orbital transitions between occupied and virtual orbitals for both molecular cases.

Considering different peak intensities of the laser field ($1.40 \cdot 10^{11}$ W/cm^2, $8.76 \cdot 10^{11}$ W/cm^2 and $2.24 \cdot 10^{12}$ W/cm^2), the molecular response of 5BU and 6BU to the laser excitation also show different pictures. For example, for the highest peak intensity 5BU excitation enters in a saturation regime after 18-19 fs, followed by a decreasing of absorption, while 6BU continuously absorbs photons from the laser field, probably saturation occurs at longer than pulse duration times. On the other hand, the smallest value of the laser field peak intensity is insufficient to have a considerable excitation for the molecules; we have obtained significant laser field absorption only for the last two peak intensity values.

Acknowledgments

This work has been supported by the Romanian National Authority for Scientific Research (ANCS) through the PN-II-RUTE-2011-3-0124 Research Project. We gratefully acknowledge the Data Center of NIRDIMT Cluj-Napoca for providing computational infrastructure and the technical assistance.

References

1 B. Wardle, *Principles and Applications of Photochemistry*, John Wiley & Sons Ltd, United Kingdom, 2009.
2 C. T. Middleton, K. de La Harpe, C. Su, Y.-K. Law, C. E. Crespo-Hernández, and B. Kohler, *Annu. Rev. Phys. Chem.*, 2006, **60**, 217–239.
3 A. Luque and S. Hegedus, *Handbook of Photovoltaic Science and Engineering*, John Wiley & Sons Ltd, United Kingdom, 2011.
4 A. McPherson, G. Gibson, H. Jara, U. Johann, T. S. Luk, I. A. McIntyre, K. Boyer, and C. K. Rhodes, J. *Opt. Soc. Am. B*, 1987, **4**, 595–601.
5 M. Ferray, A. L'Huillier, X. F. Li, L. A. Lompre, G. Mainfray, and C Manus, *J. Phys. B: At. Mol. Opt. Phys.*, 1988, **21**, L31.
6 M. F. Kling, and M. J. J. Vrakking, *Ann. Rev. Phys. Chem.*, 2011, **59**, 463–492.
7 A. H. Zewail, *The Chemical bond: structure and dynamics*, Academic Press, 1992.
8 H. Rabitz, R. de Vivie-Riedle, M. Motzkus, and K. Kompa, *Science*, 2000, **288**, 824–828.
9 R. J. Levis, G. M. Menkir, and H. Rabitz, *Science*, 2001, **292**, 709–713.
10 S. Zou, Q. Ren, G. G. Balint-Kurti, and F. R. Manby, *Phys. Rev. Lett.*, 2006 **96**, 243003.
11 T. Herrmann, Q. Ren, G. G. Balint-Kurti, and F. R. Manby, *J. Chem. Phys.*, 2007, **126**, 224309.
12 E. Runge, E. K. U. Gross, *Phys. Rev. Lett.*, 1984, **52**, 997
13 M. Petersilka, U. J. Gossmann, E. K. U. Gross, *Phys. Rev. Lett.*, 1996, **76**, 12121215.
14 M. E. Casida, In *Recent advances in density functional methods*; D. P. Chong, Ed.; World Scientific Publishing: River Edge, NJ, 1995, Vol. 1, Chapter 5, 155192.
15 C. A. Ullrich *Time-Dependent Density Functional Theory: Concepts and Applications*, Oxford University Press, Oxford New York, 2012.
16 K. Burke, J. Werschnik, E. K. U. Gross, *J. Chem. Phys.*, 2005, **123**, 062206.
17 S. Meng and E. Kaxiras, *J. Chem. Phys.*, 2008, **129**, 054110.
18 K. Lopata and N. Govind, *J. Chem. Theory Comput.*, 2011, **7**, 1344–1355.
19 K. C. Kulander, *Phys. Rev. A*, 1987, **36**, 2726–2738.
20 A. N. Markevitch, S. M. Smith, D. A. Romanov, H. B. Schlegel, M. Y. Ivanov, and R. J. Levis, *Phys. Rev. A*, 2004, **69**, 013401.
21 X. Li, S. Smith, A. Markevitch, D. Romanov, R. Levis, H. B. Schlegel, *Phys. Chem. Chem. Phys.*, 2005, **7**, 233–239.
22 H. Eshuis, G. G. Balint-Kurti, F. R. Manby, *J. Chem. Phys.*, 2008, **128**, 114113.
23 S. K. Min, Y. Cho, K. S. Kim, *J. Chem. Phys.*, 2011, **135**, 244112.
24 G. Sun, C. Fecko, R. B. Nicewonger, W. W. Webb, and T. P. Begley, *Org. Lett.*, 2006, **8**, 681–683.
25 M. Micciarelli, C. Altucci, B. Della Ventura, R. Velotta, V. Toşa, A. B. Gónzalez Pérez, M. Pérez Rodríguez, Á. R. de Lera, and Attila Bende, *Phys. Chem. Chem. Phys.*, 2013 **15**, 7161–7173.
26 M. Micciarelli, M. Valadan, B. Della Ventura, G. Di Fabio, L. De Napoli, S. Bonella, U. Rothlisberger, I. Tavernelli, C. Altucci and R. Velotta, *J. Phys. Chem. B*, 2014 **118**, 4983–4992.
27 H.-J. Werner, P. J. Knowles, G. Knizia, F. R. Manby, M. Schütz, WIREs Comput. Mol. Sci., 2012, **2**, 242–253
28 MOLPRO version 2012.1 is a package of ab initio programs written by H.–J. Werner, P. J. Knowles, G. Knizia, F. R. Manby, M. Schütz, P. Celani, T. Korona, R. Lindh, A. Mitrushenkov, G. Rauhut, K. R. Shamasundar, T. B. Adler, *et al*. see http://www.molpro.net.
29 D. A. Micha, *J. Phys. Chem. A*, 1999, **103**, 7562–7574.
30 R. Peverati, and D. G. Truhlar, *J. Phys. Chem. Lett.*, 2012, **3**, 117–124.
31 F. Weigend, R. Ahlrichs, *Phys. Chem. Chem. Phys.*, 2005 **7**, 3297–3305.
32 R. Peverati, and D. G. Truhlar, *Phys. Chem. Chem. Phys.*, 2012, **14**, 11363–11370.
33 R. Peverati, and D. G. Truhlar, *J. Phys. Chem. Lett.*, 2011, **2**, 2810–2817.
34 S. Hirata, M. Head-Gordon, *Chem. Phys. Lett.* 1999, **314**, 291–299.
35 F. R. Manby, P. J. Knowles, A. W. Lloyd, *J. Chem. Phys.*, 2001, **115**, 9144–9148.
36 GAUSSIAN09, Revision D.01, M. J. Frisch, G. W. Trucks, H. B. Schlegel, G. E. Scuseria, M. A. Robb, J. R. Cheeseman, G. Scalmani, V. Barone, B. Mennucci, G. A. Petersson, H. Nakatsuji, M. Caricato, X. Li, H. P. Hratchian, A. F. Izmaylov, J. Bloino, G. Zheng, J. L. Sonnenberg, M.

Hada, M. Ehara, K. Toyota, R. Fukuda, J. Hasegawa, M. Ishida, T. Nakajima, Y. Honda, O. Kitao, H. Nakai, T. Vreven, J. A. Montgomery, Jr., J. E. Peralta, F. Ogliaro, M. Bearpark, J. J. Heyd, E. Brothers, K. N. Kudin, V. N. Staroverov, T. Keith, R. Kobayashi, J. Normand, K. Raghavachari, A. Rendell, J. C. Burant, S. S. Iyengar, J. Tomasi, M. Cossi, N. Rega, J. M. Millam, M. Klene, J. E. Knox, J. B. Cross, V. Bakken, C. Adamo, J. Jaramillo, R. Gomperts, R. E. Stratmann, O. Yazyev, A. J. Austin, R. Cammi, C. Pomelli, J. W. Ochterski, R. L. Martin, K. Morokuma, V. G. Zakrzewski, G. A. Voth, P. Salvador, J. J. Dannenberg, S. Dapprich, A. D. Daniels, O. Farkas, J. B. Foresman, J. V. Ortiz, J. Cioslowski, and D. J. Fox, Gaussian, Inc., Wallingford CT, 2013.

37 M. J. G. Peach, P. Benfield, T. Helgaker, D. J. Tozer, *J. Chem. Phys.*, 2008, **128**, 044118.

38 M. D. Hanwell, D. E. Curtis, D. C. Lonie, T. Vandermeersch, E. Zurek, and G. R. Hutchison, *J. Cheminf.*, 2012, **4**, 17–.

39 A.-R. Allouche, *J. Comput. Chem.*, 2011, **32**, 174–182.

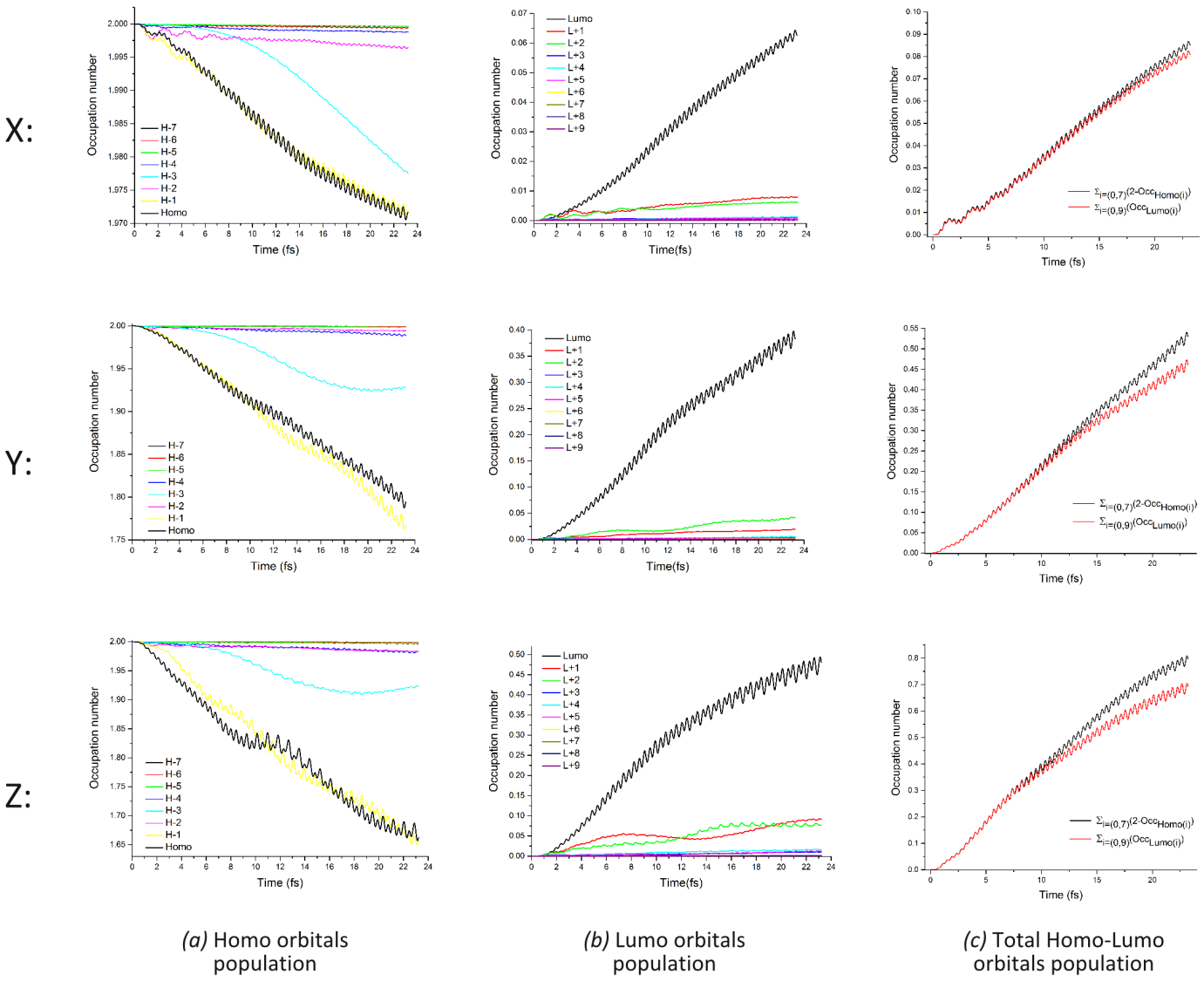

Fig. 3 Different occupied (the highest eight), virtual (lowest nine) and the total occupied-virtual orbital population induced by an oscillating field applied in the *X*, *Y*, and *Z* directions for 5BU.

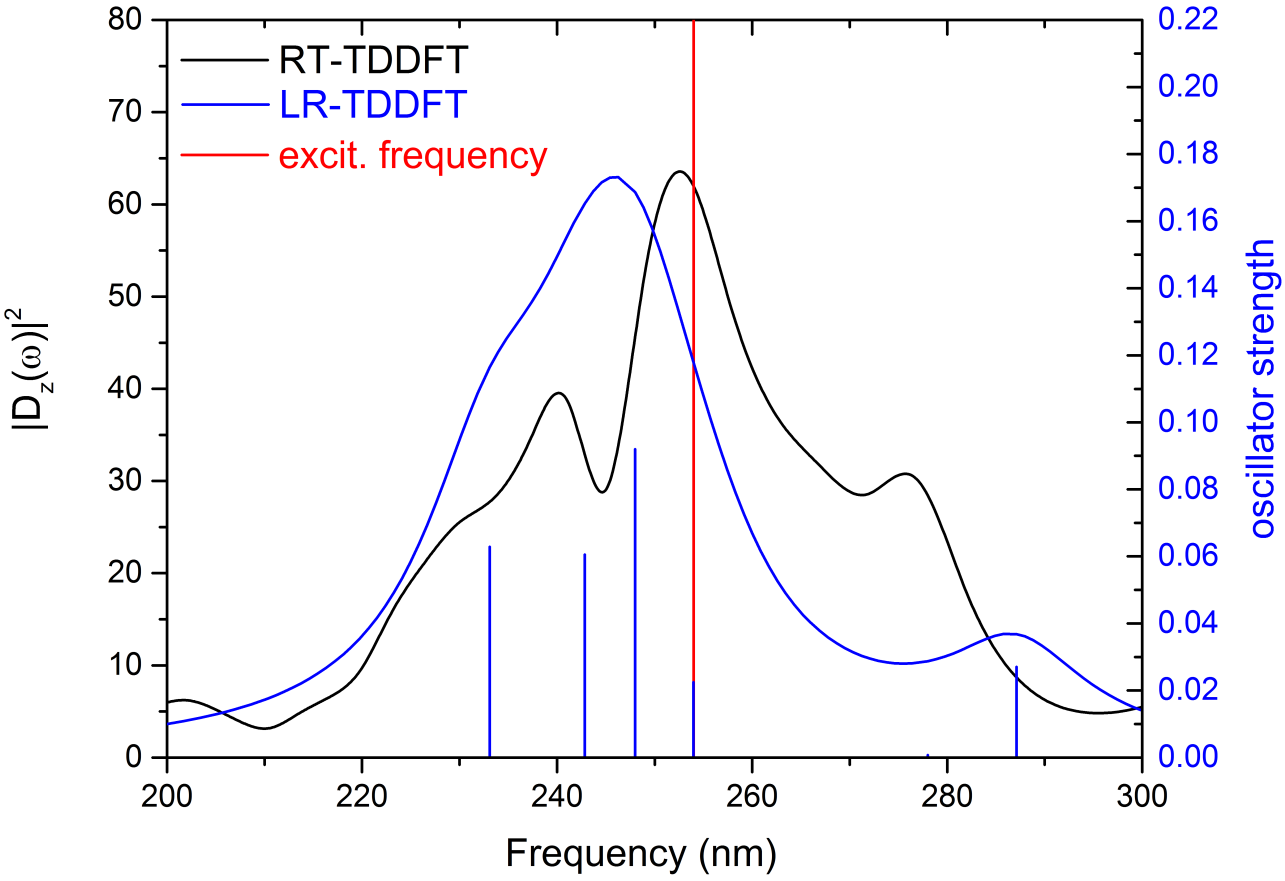

Fig. 4 The dipole moment intensity along the Z axis in frequency domain obtained with the real-time propagation theory (black line) and the excitation line of the laser field (red line), as well as the theoretical UV spectra calculated with the linear-response method (blue line) for 5BU system.

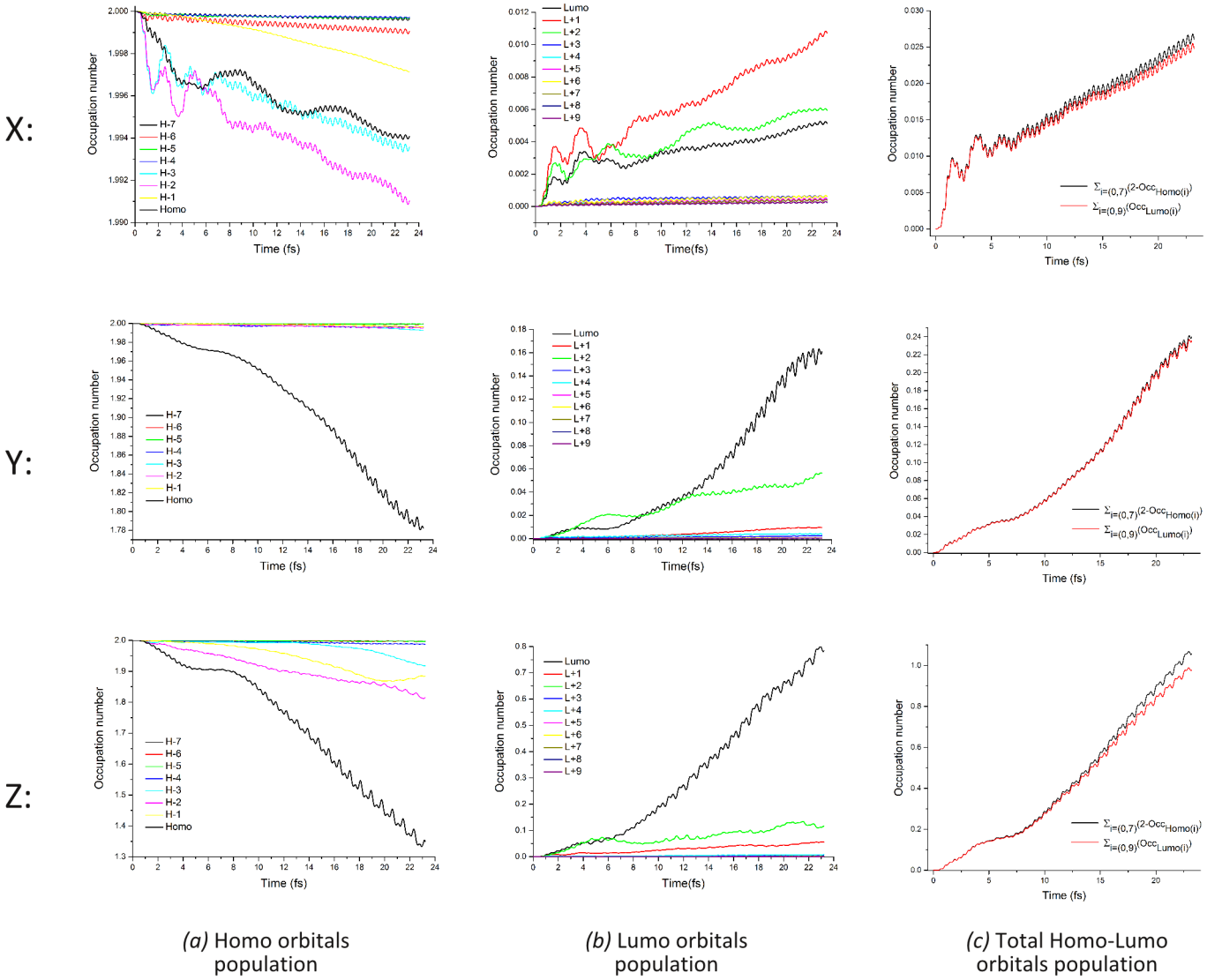

Fig. 5 Different occupied (the highest eight), virtual (lowest nine) and the total occupied-virtual orbital population induced by an oscillating field applied in the *X*, *Y*, and *Z* directions for 6BU.

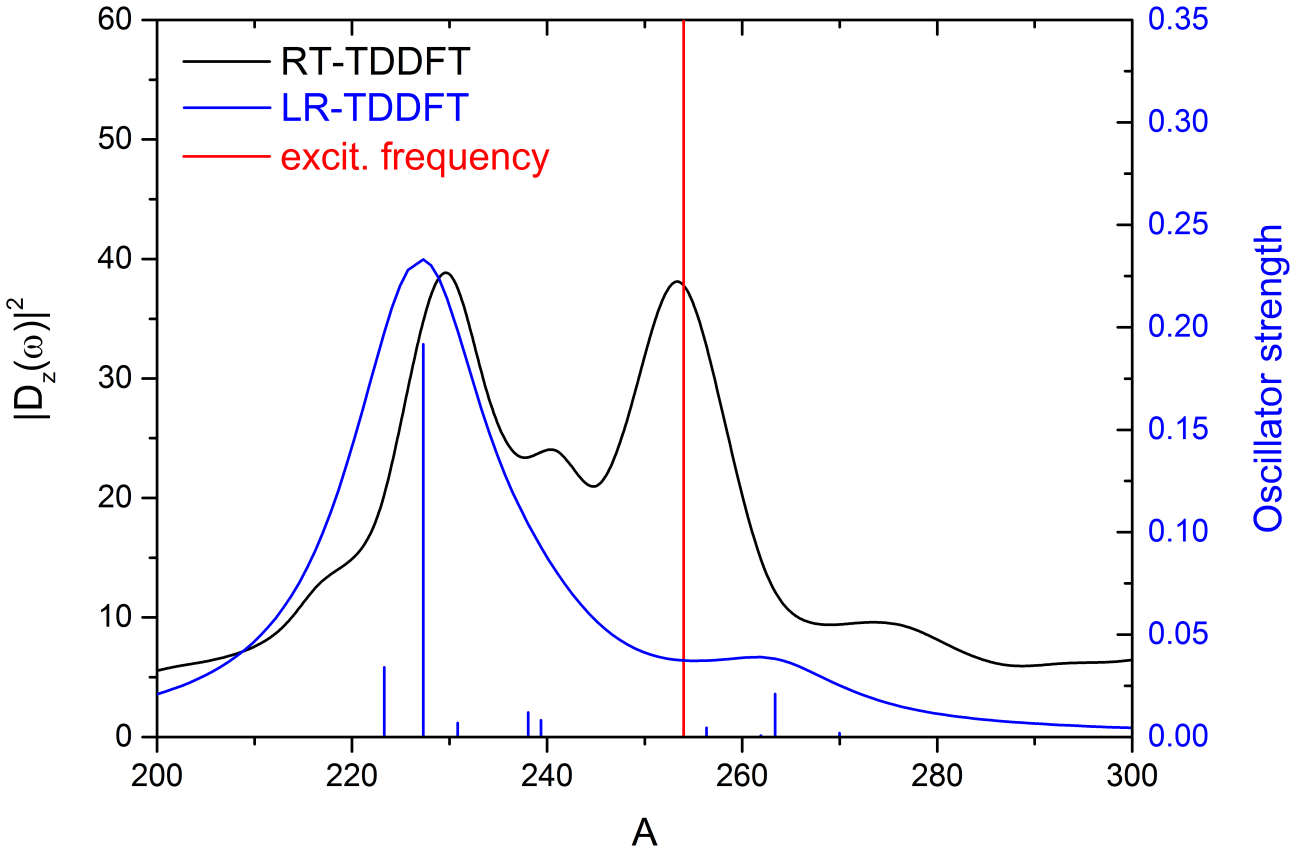

Fig. 6 The dipole moment intensity along the Z axis in frequency domain obtained with the real-time propagation theory (black line) and the excitation line of the laser field (red line), as well as the theoretical UV spectra calculated with the linear-response method (blue line) for 6BU system.

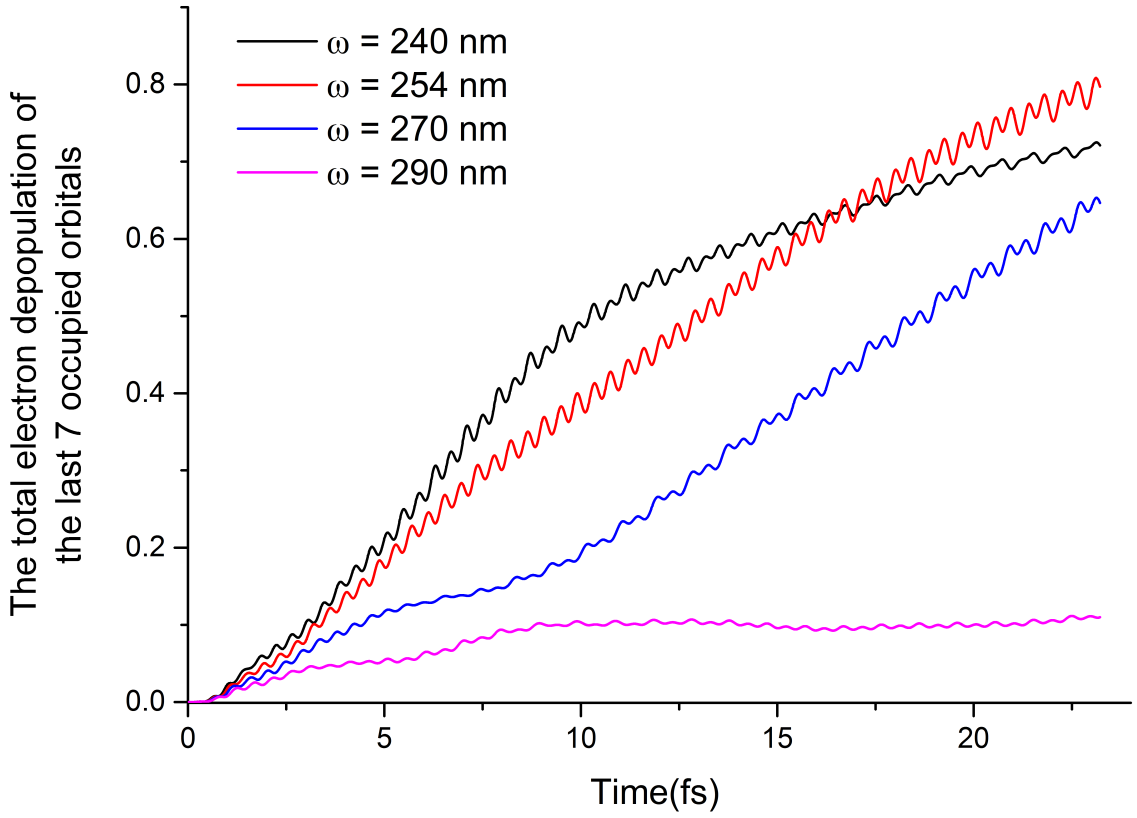

Fig. 7 The total fractional electron depopulation of the last seven occupied orbitals for 5BU using four different (240 nm, 254 nm, 270 nm and 290 nm) laser wavelengths in the direction of *Z* axis.

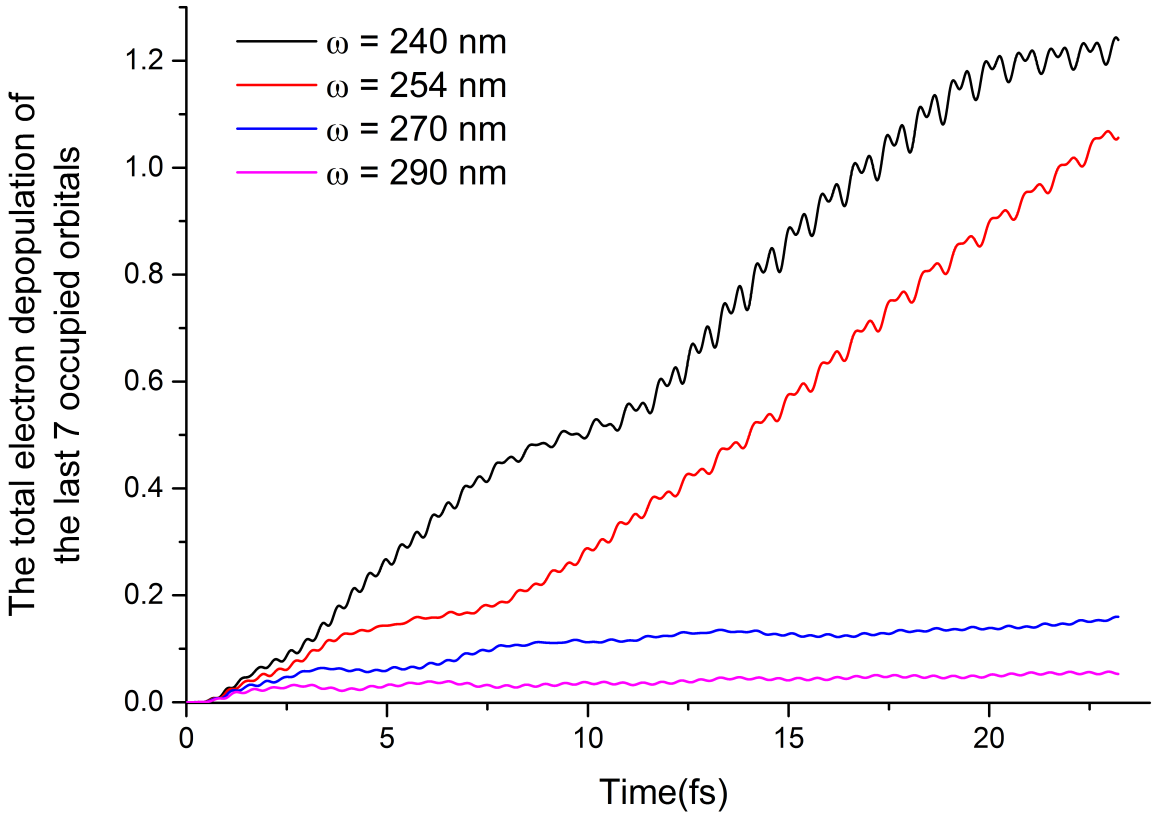

Fig. 8 The total fractional electron depopulation of the last seven occupied orbitals for 6BU using four different (240 nm, 254 nm, 270 nm and 290 nm) laser wavelengths in the direction of *Z* axis.

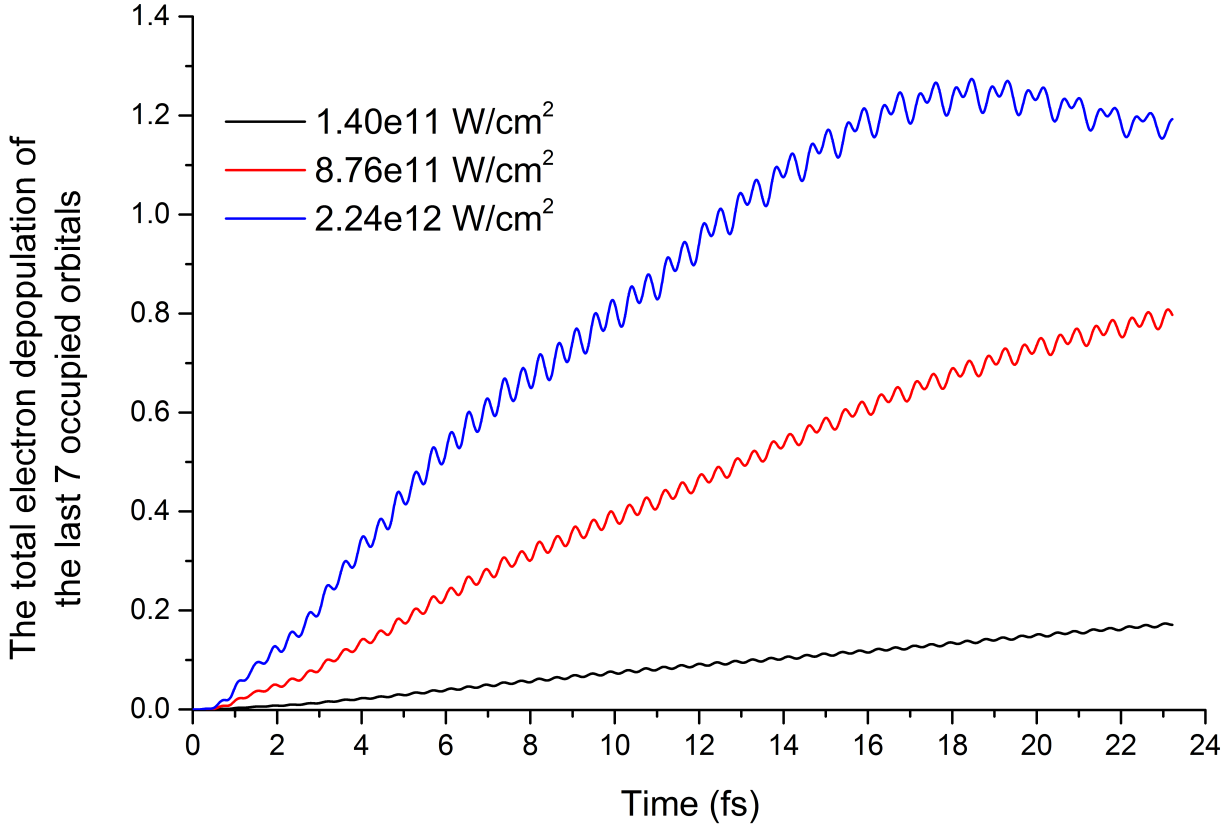

Fig. 9 The total fractional electron depopulation of the last seven occupied orbitals for 5BU using three different ($1.40 \cdot 10^{11}$, $8.76 \cdot 10^{11}$ and $2.24 \cdot 10^{12}$ W/cm^2) laser intensities in the direction of Z axis.

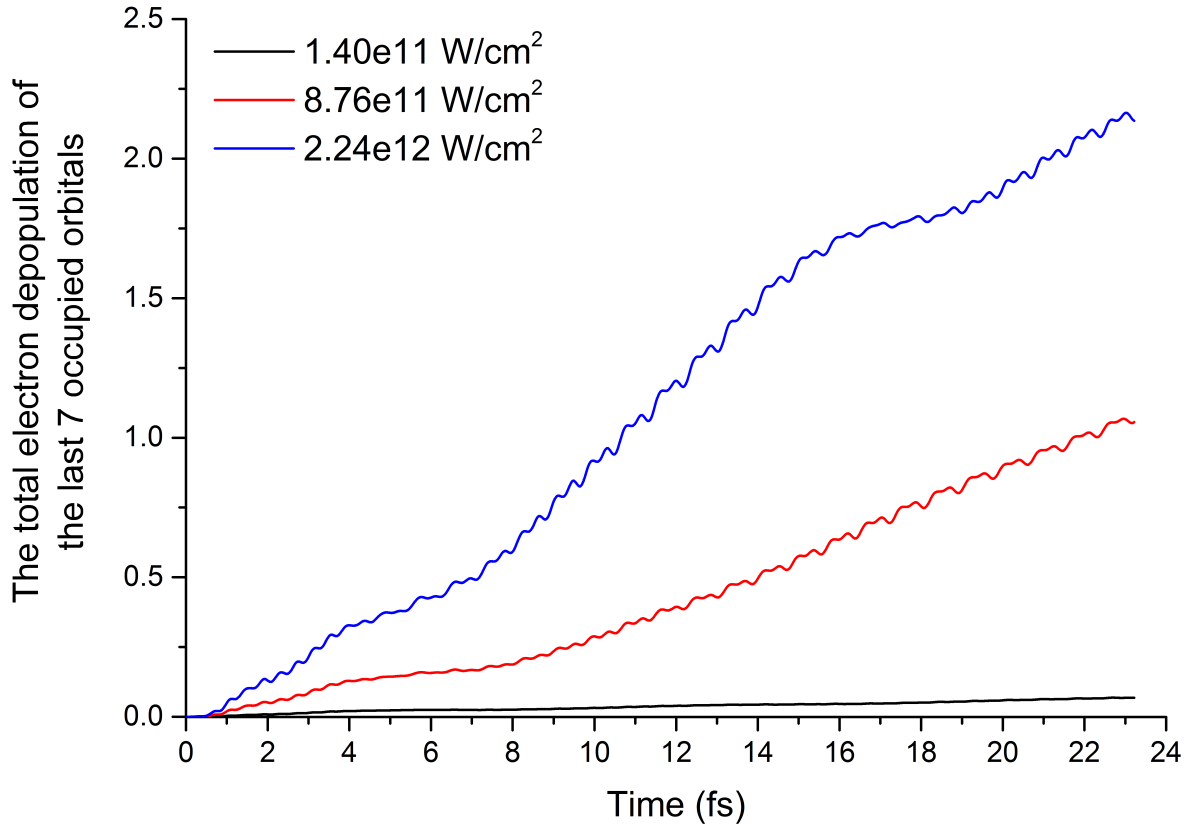

Fig. 10 The total fractional electron depopulation of the last seven occupied orbitals for 6BU using three different ($1.40 \cdot 10^{11}$, $8.76 \cdot 10^{11}$ and $2.24 \cdot 10^{12}$ W/cm^2) laser intensities in the direction of Z axis.